Three-dimensional velocity field of present-day crustal motion of the Tibetan Plateau derived from GPS measurements

Shiming Liang,[1] Weijun Gan,[1] Chuanzheng Shen,[1] Genru Xiao,[2] Jing Liu,[3] Weitao Chen,[4] Xiaoguang Ding,[1] and Deming Zhou [1]

Received 7 July 2013; revised 2 October 2013; accepted 7 October 2013; published 24 October 2013.

[1] Using the measurements of 750 GPS stations around the Tibetan Plateau for over 10 years since 1999, we derived a high-resolution 3-D velocity field for the present-day crustal movement of the plateau. The horizontal velocity field relative to stable Eurasia displays in details the crustal movement and tectonic deformation features of the India-Eurasia continental collision zone with thrust compression, lateral extrusion, and clockwise rotation. The vertical velocity field reveals that the Tibetan Plateau is continuing to rise as a whole relative to its stable north neighbor. However, in some subregions, uplift is insignificant or even negative. The main features of the vertical crustal deformation of the plateau are the following: (a) The Himalayan range is still rising at a rate of ~2 mm/yr. The uplift rate is ~6 mm/yr with respect to the south foot of the Himalayan range. (b) The middle eastern plateau has a typical uplift rate between 1 and 2 mm/yr, and some high mountain ranges in this area, like the Longmen Shan and Gongga Shan, have surprising uplift rates as large as 2–3mm/yr. (c) In the middle southern plateau, there is a basin and endorheic subregion with a series of NS striking normal faults, showing obvious sinking with the rates between 0 and -3 mm/yr. (d) The present-day rising and sinking subregions generally correspond well to the Cenozoic orogenic belts and basins, respectively. (e) At the southeastern corner of the plateau. There is an apparent trend that the uplift rate is gradually decreasing from between 0.8 and 2.3 mm/yr in the inner plateau to between -0.5 and -1.6 mm/yr outside the plateau, with the decrease of terrain height.

Citation: Liang, S., W. Gan, C. Shen, G. Xiao, J. Liu, W. Chen, X. Ding, and D. Zhou (2013), Three-dimensional velocity field of present-day crustal motion of the Tibetan Plateau derived from GPS measurements, *J. Geophys. Res. Solid Earth*, *118*, 5722–5732, doi:10.1002/2013JB010503.

1. Introduction

[2] The collision and continuous convergence of India and Eurasia since the Eocene epoch (~55 Ma) have not only uplifted the Tibetan Plateau to become the "top of the world" with an average elevation of ~4500 m, covering an area of over 2.5 million km^2 but also have had a large impact on the climate, environment, and ecology of Asia and the world [*Molnar and Tapponnier*, 1975; *Rowley*, 1996].

[3] Regarding the space-time evolution characteristics of the uplift and spread of the Tibetan Plateau, although the models of noncoeval uplift in all areas and of episodic uplift have been generally accepted, their details remain highly debatable. For example, *Chung et al*. [1998], based on the difference in eruption time of K-rich lavas in east and west Qiangtang, suggested that the plateau rose first in east and then in west, while *Xu et al*. [1999] and *Tapponnier et al*. [2001] proposed a three-stage south to north growth model for the evolution of the Tibetan Plateau, in which each stage is characterized by gradual uplift and spreading of 300 to 500 km wide crustal thrust sheets. Recently, *Wang et al*. [2008a] argued that the central part of the plateau rose first and then the outer parts, based on the evidence that while the Lhasa and Qiangtang terranes, the central parts of the plateau, had risen to current elevation in the middle Eocene (~40 Ma), the Himalayas and western plateau still remained under the ocean and the northern part in the lowland. There are many disagreements in the models and conclusions about the Tibetan Plateau for two important reasons: First, the uplift history of the Tibetan Plateau is long and complex. Many previous studies, especially early works, focused on records at local places or few sites, without considering regional differences. So it is hard to

Additional supporting information may be found in the online version of this article.

[1]State Key Laboratory of Earthquake Dynamics, Institute of Geology, China Earthquake Administration, Beijing, China.
[2]Department of Geodesy, Donghua University of Technology, Jiangxi, China.
[3]Institute of Tibetan Plateau Research, Chinese Academy of Sciences, Beijing, China.
[4]National Earthquake Infrastructure Service, China Earthquake Administration, Beijing, China.

Corresponding author: W. Gan, State Key Laboratory of Earthquake Dynamics, Institute of Geology, China Earthquake Administration, Qijiahuozi St., Chaoyang District, Beijing 100029, China. (wjgan@gps.gov.cn)

2169-9313/13/10.1002/2013JB010503

arrive at a robust conclusion. Second, many parameters of plateau uplift, such as time, periods, rates, and heights, were determined based on some suppositions such as that when the plateau rises to a certain height, thickness of the lithosphere, and surface environments, including tectonics, climate, ecology, sediments, and temperature, would change notably, and from these variations, the time of plateau uplift could be estimated. Such inferences are uncertain or may even be contradictory. For example, *England and Housemen* [1989] suggested that when the Tibetan Plateau reaches its maximum elevation, convective instability of the lower lithosphere will be sufficient for E-W extension to replace N-S compression as the dominant feature of the stress field. From this, *Harrison et al*. [1995] inferred that the whole plateau had reached its current altitude at ~8Ma in terms of the formation time of the N-S directed graben in southern Tibet. However, some studies pointed out that the occurrence of E-W extension of southern Tibet is not necessarily coincident with the maximum elevation. [e.g., *McCaffrey and Nabelek*, 1998; *Lee et al*., 2003; *Kapp and Guynn*, 2004].

[4] From above, we can see that in order to obtain a more reliable model to describe the tectonic process and mechanical evolution of the Tibetan Plateau, many more observations, investigations, and constraints with high spatiotemporal resolution are indispensable. Since the middle 1990s, a wealth of GPS measurements has been conducted around the Tibetan Plateau. These observations allow us to put quantitative constraints on the kinematic models of the Tibetan Plateau. For instance, for the first time, *Wang et al*. [2001] presented a crustal motion velocity field using 362 GPS stations in mainland China showing a clockwise rotation of the Tibetan Plateau around the Eastern Himalayan Syntaxis and a general linear trend of GPS velocity gradient in India-Eurasia convergence direction, as well as the feature that the eastern component of all GPS velocities become larger for stations located further east relative to stable Eurasia. *Zhang et al*. [2004], using 553 GPS velocities around the Tibetan Plateau and decomposing the velocities in the direction of India-Eurasia convergence, revealed that the decreases of linear gradients from south to north can be best described by the continuum deformation model. *Gan et al*. [2007], using 726 GPS velocities around the Tibetan Plateau, highlighted the interior deformation within the plateau by removing the rigid motion of the entire plateau and demonstrated that the most remarkable interior deformation of the plateau is a "glacier-like flow" zone which starts at the middle and western plateau, goes clockwise around the Eastern Himalayan Syntaxis, and ends at the southeast corner of the plateau with a fanlike front. The emergence of the flow zone could be attributed to an eastward escape of highly plastic upper crustal material driven by a lower crust viscous channel flow [*Royden et al*., 1997].

[5] It is noted that so far, most studies on crustal motion and deformation based on GPS observations have focused on horizontal velocities. The use of vertical velocities is still challenging because the vertical positioning precision of GPS measurements is typically about 2–2.5 times lower than that of the horizontal. Furthermore, vertical velocity of crustal motion or deformation is usually remarkably small compared to the horizontal one. Thus, GPS measurements with a short time span are of little value in estimating reliable vertical crustal deformation. However, with a long time span of observations, the cumulative vertical crustal deformation can exceed the random errors of GPS measurements and it becomes possible to acquire reliable vertical crustal deformation. For example, *Devoti et al.* [2010] obtained a high-resolution image of vertical deformation of Italy and its surroundings with the GPS measurements from 1998 to 2008. Similarly, *Beavan et al*. [2010] derived a 3-D velocity field of crustal motion for the Southern Alps in New Zealand by means of a 10 year span of GPS data.

[6] In this work, we use GPS data collected at 750 stations around the Tibetan Plateau since 1999 to obtain a 3-D velocity field for the present-day crustal motion of the plateau with high resolution. This 3-D velocity field provides a better understanding of the tectonic deformation process on the Tibetan Plateau as well as important kinematic constraints on the dynamics of the present-day uplifting and spreading of the plateau.

2. GPS Data and Data Processing

2.1. GPS Data

[7] During the last two decades, a large number of GPS measurements have been carried out in mainland China. Among them, two national major projects implemented by the China Earthquake Administration and other collaborating organizations are most notable. One is the Crustal Movement Observation Network of China (CMONOC I) [*Niu et al*., 2005], which has 27 continuously operating GPS stations and 1056 campaign-mode GPS stations. Of these, 11 continuous stations and 422 campaign stations are located around the Tibetan Plateau. Another is the Tectonic and Environmental Observation Network of Mainland China (CMONOC II) [*Gan et al*., 2012], which added 233 continuous stations and 1000 campaign-mode stations successively to the CMONOC I network. Of these, 130 continuous stations and 165 campaign-mode stations are located around the Tibetan Plateau. In addition, some institutions in China and abroad have conducted GPS observations around the Tibetan Plateau. For example, California Institute of Technology (Caltech) deployed 12 continuous stations in the south face of Himalayas, and Institute of Tibetan Plateau Research, Chinese Academy of Sciences (ITPCAS) deployed 5 continuous stations in southern Tibet. The data used in this work are taken from the sources listed in Table 1, and the locations of the GPS stations are shown in Figure 1. In the two national projects aforementioned, all campaign-mode GPS stations have reinforced concrete monuments with forced-centering apparatus for GPS antennas (Figure 2). In each survey, dual-frequency GPS receivers and choke ring antennas were used, with an occupation of at least 3 days for each station, to ensure the quality of the data. As most of the stations have at least five observational campaigns and over 10 year span (Table 1), we were able to obtain high-accuracy horizontal velocities as well as reliable vertical velocities.

2.2. Data Processing

[8] GPS data were processed with the software GPS Inferred Positioning System (GIPSY)/Orbit Analysis and

Table 1. GPS Data Around the Tibetan Plateau Used in This Work

Station	Number	Time Span	Surveying Mode	Organization
Continuous Stations of CMONOC I	11	1998–2013	Sampling rate: 30 s	China Earthquake Administration
Continuous Stations of CMONOC II	130	2010–2013	Sampling rate: 30 s	China Earthquake Administration
Continuous Stations of Caltech and ITPCAS in southern Tibet and Nepal	17	2007–2012	Sampling rate: 30 s	Caltech andITPCAS
Campaign-mode stations of CMONOC I	422	1999–2011	Sampling rate: 30 s, observed in 1999, 2001, 2004, 2007, 2009, and 2011, with an occupation of at least 3 days for each station	China Earthquake Administration
Campaign-mode stations of CMONOC II	165	2009–2011	Sampling rate: 30 s, observed in 2009 and 2011, with an occupation of at least 3 days for each station	China Earthquake Administration

Simulation Software (OASIS) (Version 6.0) [*Webb and Zumberge*, 1993] from Jet Propulsion Laboratory (JPL), NASA, using the Precise Point Positioning (PPP) strategy [*Zumberge et al*., 1997] and JPL products to obtain daily loosely constrained solutions. Then, we used the software Quasi-Observation Combination Analysis (QOCA) of JPL [*Dong et al*., 1998, 2006] to perform joint adjustment for the daily loosely constrained solutions of all stations to get their coordinate time series and optimum estimations of velocity in International Terrestrial Reference Frame (ITRF)2008. The specific procedures are described below.

[9] The linear combinations reducing or eliminating the effect of ionospheric delay are taken as observational variables. The satellite truncation elevation angle is 15°, and the data sampling rate is 300 s. Fixed International GNSS Service (IGS) 08-based precise orbits and clocks from JPL are adopted (http://sideshow.jp1.nasa.gov). The a priori global pressure and temperature model (GPT) and global-mapping function (GMF) are used [*Boehm et al*., 2006]. Correction for ocean tide loading is made with the Finite Element Solution (FES) 2004 model with online calculation (http://holt.oso.chalmers.se/loading), in the center of mass of the Earth system frame [*Scherneck et al*., 2000; *Fu et al*., 2012]. During data processing, the self-consistency of the products is taken into consideration, such as the orbits, clock difference, satellite-dependent differential code biases, phase center of receiver antenna, and phase center of satellite [*Schmid et al*., 2007]. The estimation parameters include station coordinates, clock errors of receivers, and troposphere delay. To improve solution accuracy, we apply the Ambizap software [*Blewitt*, 2008] for phase ambiguity resolving, in which various linear combinations of observational parameters are determined using the fixed point theorems, and the unique and self-consistent daily solutions with phase ambiguity resolved are generated in the end. Finally, through seven parameter transform, the daily solutions are converted into the ITRF2008 reference system.

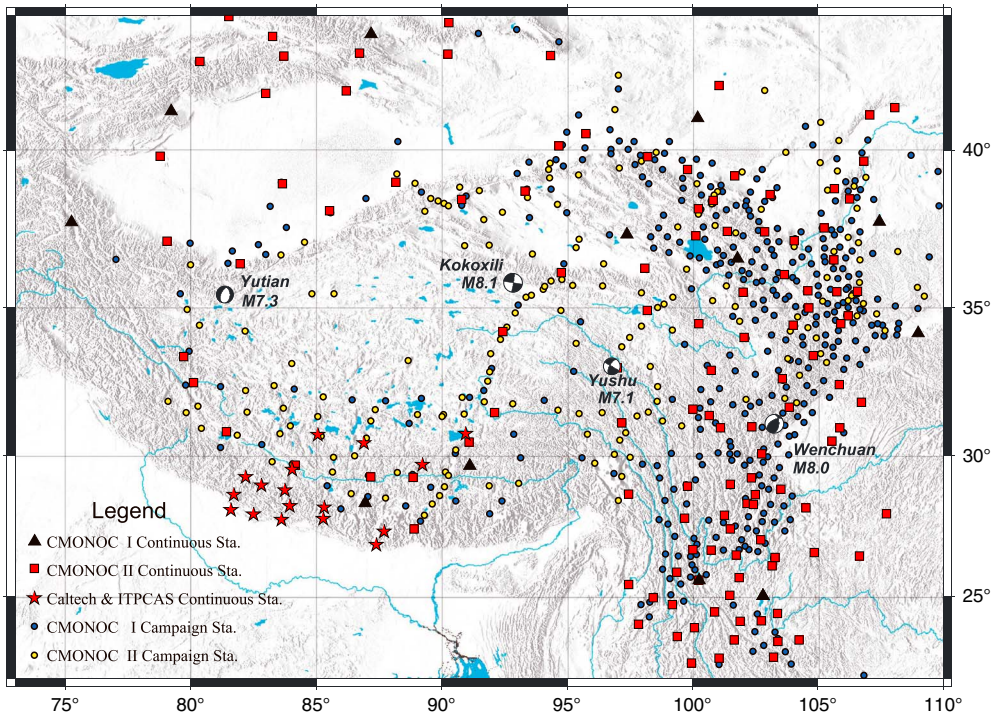

Figure 1. Map showing locations of GPS stations around the Tibetan Plateau relevant to this work and four great earthquakes occurred in the plateau during the GPS observation periods between 1999 and 2013.

Figure 2. Photo showing the monument of a typical campaign-mode GPS station of the CMONOC project, with a choke ring GPS antenna.

[10] After the above processing, we further use the 6 h global surface pressure field with a resolution of 2.5°from National Centers for Environmental Prediction (NCEP) and *Farrell*s [1972] elastic Green's functions to determine nontectonic crustal deformation caused by atmospheric loading [*Tregoning and Watson*, 2009]. Considering that insufficient sampling in the atmospheric pressure field could cause a fractional tidal component [*Tregoning and van Dam*, 2005], we applied the 20 order Butterworth low-pass filter to the atmospheric loading time series to delete these residual tidal components [*Tregoning and Watson*, 2009] before using them to correct the GPS position time series.

[11] In order to remove other nontectonic crustal deformation sources of noise, such as annual variations of surface water loading, on campaign-mode stations, we derived an annual wave function for each continuous GPS station from its vertical coordinate variation time series and used the annual wave functions to perform nontectonic deformation correction to the vertical coordinate variations of all campaign-mode stations, based on the assumption that the effect of nontectonic crustal deformation for GPS stations is spatially correlated. The more detailed strategy is as follows: First, we choose some continuous GPS stations which should have observation time spans over 2.5 years and capability to yield reliable estimations of annual wave functions via their time series to construct a Delaunay triangle network. Then, for a given campaign-mode station, we interpolate its annual wave function based on the annual wave functions of the three continuous stations of its corresponding Delaunay triangle and the algorithm of inverse-distance weighted average. And then, using the annual wave function, we calculate the correction values of vertical nontectonic deformation for this station on the specific days when GPS observations were carried out. The result shows that such a correction can significantly reduce the divergence of the time series of the campaign-mode stations and improve the accuracy of vertical velocity estimation, especially for those stations with few observations (less than three campaigns) and short observation time spans. Figure 3 displays a comparison of the time series of vertical coordinates for some typical campaign-mode stations before and after the annual wave function-based nontectonic deformation correction.

[12] Finally, we use the QOCA software [*Dong et al.*, 1998, 2006] to perform adjustment on the daily loosely constrained solutions for all GPS stations in Tibet, together with 124 IGS tracking stations in the world. The QOCA modeling of the data was done through sequential Kalman filtering, allowing adjustment for global translation and rotation of each daily solution. It also allowed re-estimation of sigma for GPS stations with two optional noise analysis models: white noise model and flick noise + white noise model. In this work, we used white noise model for campaign-mode GPS stations and flick noise + white noise model for continuous GPS stations.

[13] It is noted that four great earthquakes, that is, the 14 November 2001 Kokoxili M8.1earthquake, 21 March 2008 Yutian M7.3 earthquake, 12 May 2008 Wenchuan M8.0 earthquake, and 14 April 2010 Yushu M7.1 earthquake (Figure 1), occurred around the Tibetan Plateau during our observation periods between 1999 and 2013. We removed the effects of the Kokoxili M8.1, Yutian M7.3,

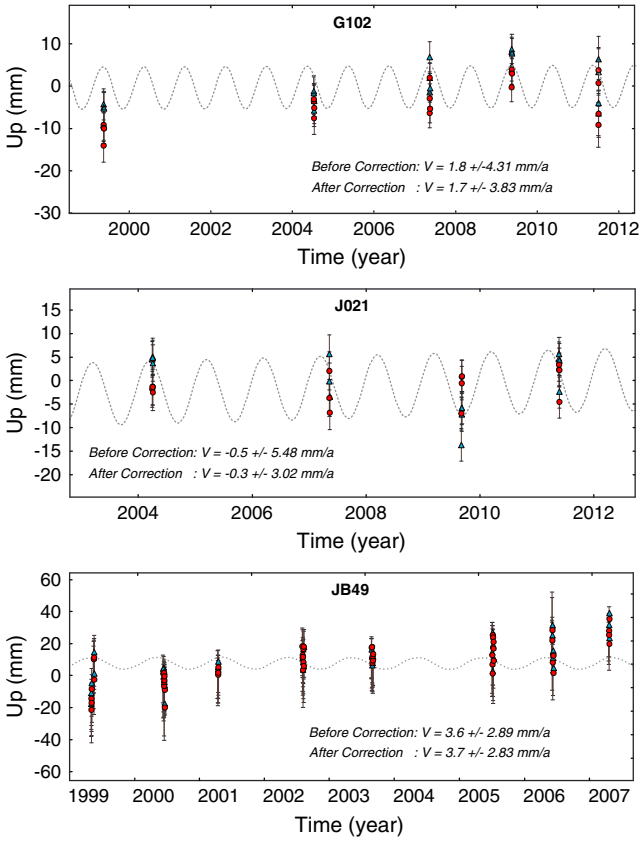

Figure 3. Comparison of time series of vertical coordinates for some typical campaign-mode stations before and after the annual wave function-based nontectonic deformation correction. Blue triangle: before correction; Red dot: after correction; Dashed gray curve: annual variation of nontectonic deformation. The errors bars represent 2 standard deviations on either side of the plotted points.

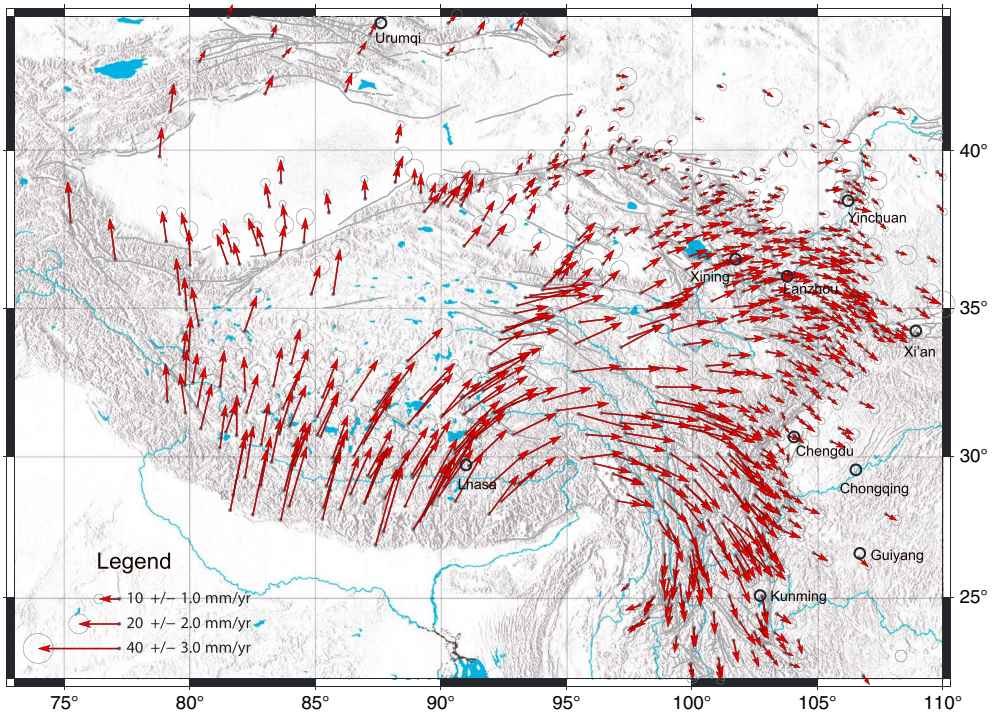

Figure 4. Horizontal GPS velocities of crustal motion around the Tibetan Plateau relative to stable Eurasia. The light gray ellipse at the tip of each velocity vector is 95% confidence. The thick gray solid lines indicate active faults in Holocene [*Deng et al*., 2003].

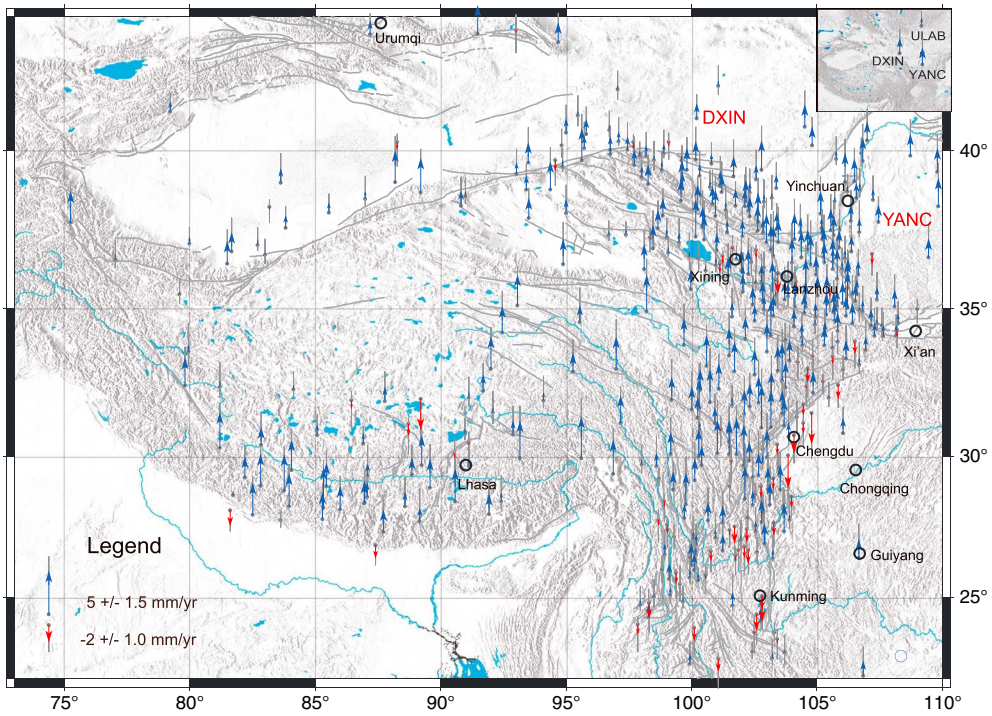

Figure 5. Vertical GPS velocities of crustal motion around the Tibetan Plateau relative to ITRF2008. Blue vectors denote uplift and red vectors denote decline. The light gray error bar at the tip of each velocity vector represents 1 standard deviation. The submap shows three continuous GPS stations, DXIN, YANC, and ULAB, which are located in the stable blocks northeast of the Tibetan Plateau and have reliable vertical velocity estimations with observation time span over 12 years. The thick gray solid lines indicate active faults in Holocene [*Deng et al*., 2003].

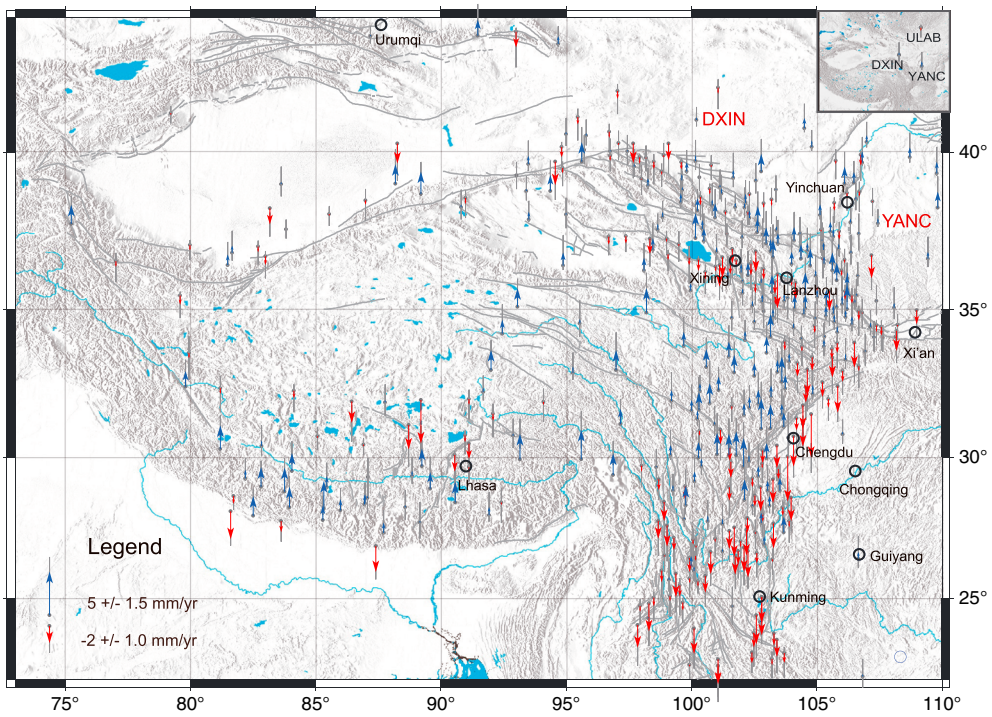

Figure 6. Vertical GPS velocities of crustal motion of the Tibetan Plateau relative to more stable surroundings to the north represented by three continuous stations, DXIN, YANG, and ULAB northeast of the plateau (in submap). Blue vectors denote uplift and red vectors denote decline. The light gray error bar at the tip of each velocity vector represents 1 stand deviations. The thick gray solid lines indicate active faults in Holocene [*Deng et al*., 2003].

and Yushu M7.1 earthquakes on the relevant GPS stations by using the coseismic module in the QOCA software. The detailed procedure is as follows: First, the Faultview module of QOCA was used to calculate the coseismic displacement of each GPS station based on an elastic half-space dislocation model [*Okada*, 1992] and a priori coseismic slip distributions of these events [*Wan et al*., 2004; *Zhang et al*., 2011b; *Jiang et al*., 2013; *Sun et al*., 2013], which are represented by a series of dislocated finite rectangular fault patches. Then, for the stations whose coseismic displacement estimates are equal or greater than 3 mm, we added three coseismic displacement parameters when solving the velocity field. Thus, the final coseismic displacement of the stations was actually calculated with an improved coseismic slip distribution model which was optimally estimated as part of the velocity fitting process. The impact from the postseismic displacements of the three events was not considered in the data processing because it was relatively small. As for the 2008 Wenchuan M8.0 earthquake, considering that a lot of stations are closely located around the rupture zone of the great event, with their coseismic displacements as large as 0.5 ~ 2.4 m [*Wang et al*., 2001], plus the fact that the postseismic deformation around the stations is still significant so far, we are not able to remove the effects of coseismic and postseismic displacements to these stations with an acceptable accuracy and thus excluded the data of these stations observed after May 2008.

[14] Finally, on the assumption that the 3-D coordinates of all stations change linearly with time, we estimate their coordinates, optimal 3-D velocities, and corresponding standard deviations in ITRF2008 reference frame. The data are listed in supporting information.

3. Three-Dimensional Velocity Field of Crustal Motion in the Tibetan Plateau

[15] Figures 4 and 5 display the present-day horizontal and vertical GPS velocity field of crustal motion in the Tibetan Plateau, respectively. Notice that the number of vertical velocity vectors is merely 450, much less than that of horizontal velocity vectors. The reason is that the observation time spans of some stations are too short to determine their vertical velocities reliably. We removed the vertical velocity vectors of the stations whose observation time spans are less than 3 years and the standard deviations (1σ) of vertical velocity are larger than 2.5 mm/yr. Besides, the Qiangtang and Kokoxili areas in the central and western plateau remain gaps in the coverage of our GPS network because of atrocious environmental conditions for field work.

[16] From the horizontal velocity field relative to stable Eurasia in Figure 4, we can see that the Indian plate is pushing the Eurasia along the Himalayas in NNE direction at a rate of ~ 40 mm/yr. The velocity of Tibetan crust slows down sharply from south to north, causing strong shortening between India and Eurasia, as well as apparent lateral extruding. Especially in the southeastern plateau, the velocities exhibit conspicuous clockwise rotation around the Eastern Himalayan Syntaxis and present a fanlike front at the southeast corner of the plateau. The velocity pattern explicitly reflects strong lateral extrusion and continuous deformation of the Tibetan upper crust and has been discussed by previous

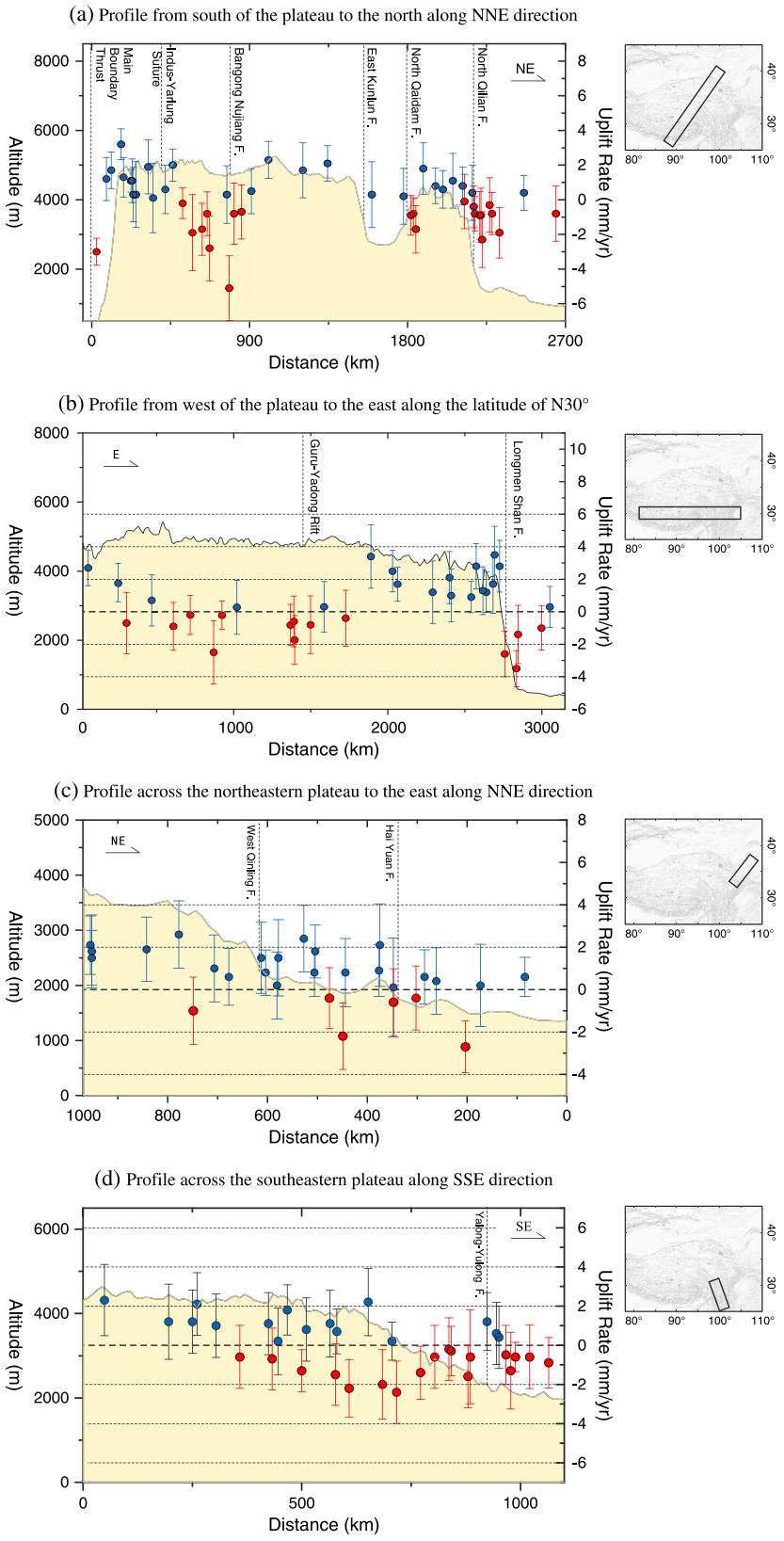

Figure 7. Profile charts showing the terrain height and uplift rate of the Tibetan Plateau. The blue dots with error bar denote GPS sites with positive uplift rates and the red dots with negative rates. The errors bars represent 2 standard deviations on either side of the plotted points.

researchers [e.g., *Wang et al*., 2001; *Zhang et al*., 2004; *Thatcher*, 2007; *Gan et al*., 2007].

[17] The vertical GPS velocities in Figure 5 are relative to ITRF2008, which was established by using the reprocessed solutions of about 580 stations around the world with observations of at least one of the four space geodetic techniques, VLBI, SLR, GPS, and DORIS, and realized the latest International Terrestrial Reference System [*Altamimi et al*., 2011]. The origin of ITRF2008 is the Earth center of mass, including oceans and the atmosphere. Thus, the vertical velocities in Figure 5 represent the motion of the Tibetan Plateau and its surroundings with respect to the current Earth center. Nevertheless, due to some small but systematic errors in determination of the Earth center and ITRF2008, the resultant vertical velocities are not merely associated with tectonic movement. In order to highlight the uplift of the plateau relative to its stable neighbor to the north, we choose three continuous GPS stations DXIN, YANC, and ULAB (Figures 5 and 6) as reference points to subtract the weighted average of the vertical velocities of the three stations from the vertical velocity field in ITRF2008. These three stations are located in Alashan block, Ordos block, and Mongolia block, northeast of the plateau, respectively, and all of them have been observed over 12 years and their position time series present ideal linear features. The weighted average of the vertical velocities of the three stations in ITRF2008 is 1.41 ± 0.41 mm/yr. Here the uncertainty ($\sigma = 0.41$ mm/yr) will be propagated into the uncertainties of all sites relative to the stable block to the north (See Table S1 in the supporting information). Figure 6 shows the vertical velocity field of the Tibetan Plateau relative to the stable block to the north.

[18] In Figure 6, we can quantitatively see that the Tibetan Plateau is continuing to rise as a whole relative to the block to the north. However, in some areas, uplift is insignificant or even negative. The sinking areas generally correspond to Cenozoic basins with low relief. More detailed features can be identified from the profile charts in Figure 7, as follows:

[19] 1. The Himalayan range with average altitude of ~6000 m is continuing to uplift at a rate of ~2 mm/yr, and the uplift rate is ~6 mm/yr with respect to the south foot of Himalayan range, which means that the Himalayan range is still rising intensively with the underthrusting of the Indian plate (Figures 6 and 7a). In addition, the middle eastern plateau is another area with a typical uplift rate between 1 and 3 mm/yr, and for some high mountain ranges in this area, like the Longmen Shan and Gongga Shan, the uplift rates are as fast as 2–3 mm/yr (Figures 6 and 7b).

[20] 2. In the middle southern plateau, there is a region with a size of ~500 km × 1500 km, showing obvious decline with the rates between 0 and −3 mm/yr (Figures 6, 7a, and 7b). The region, located in front of the north foothills of the Himalayan Mountains, is undergoing apparent transverse extension characterized by NS striking normal faults [*Chen et al*., 2004; *Gan et al*., 2007]. It is also an endorheic region with hundreds of lakes [*Yao*, 2008; *Ma et al*., 2011]. In the profile charts of uplift and topography (Figures 7a and 7b), we can see that that the sinking region inferred from present-day GPS measurement exactly corresponds to a basin area.

[21] 3. Along a NNE striking profile of the plateau (Figure 7a), most of the orogenic belt regions, between the Himalayas and the Indus-Yarlung suture zone, Bangong-Nujiang suture zone to East Kunlun fault, and North Qaidam fault to North Qilian fault, show apparent uplift, with typical rates between 0 and 2 mm/yr. Whereas the basin regions along the middle southern plateau, north margin of the Qaidam basin and Hexi Corridor basin present significant or insignificant decline. Thus, it can be concluded that the present-day uplifting and sinking regions correspond well with the Cenozoic orogenic belts and basins, respectively.

[22] 4. In the northeastern plateau, along a NE striking profile across West Qinling fault, Haiyuan fault, and the northeastern boundary of the plateau to Ordos block, the terrain height decreases dramatically from ~4000 m to ~1500 m. Meanwhile, the uplift rate decreases from ~2 mm/yr to less than 1 mm/yr (Figure 7c). Comparing with the uplift difference between the Qilian Shan and Hexi Corridors in northeastern plateau, we can see that the eastern part of the northeastern plateau has a gentle trend of decline at a large scale of ~1000 km (Figures 7a and 7c).

[23] 5. At the southeastern corner of the plateau, while the horizontal velocity field demonstrates a marked clockwise rotation and fanlike front of a flow zone [*Gan et al*., 2007] (Figure 4), the vertical velocity field also shows significant motion difference from the inner plateau to the outside plateau (Figure 6), with an apparent trend that the uplift rate is gradually decreasing from between 0.8 and 2.3 mm/yr in the inner plateau to between −0.5 and −1.6 mm/yr outside the plateau, with the decrease of terrain height (Figure 7d).

4. Discussion

[24] Since 1924, when E. Argand first hypothesized that India slid beneath southern Eurasia forming a thick crust and high topography, numerous studies have been made on this subject and tens of competing models have been proposed to explain the tectonic processes and mechanical evolution of the uplift of the Tibetan Plateau. These models can be classified into four major categories: (1) Double Crust entails the wholesale underthrusting of Indian continental crust beneath the Tibetan Plateau and the subsequent uplift due to increasing volume and mantle buoyancy [e.g., *Argand*, 1924; *Powell*, 1986]. (2) Continental Extrusion, rather than involve the India plate underthrusting below Tibet in large scale, explains the shortening, thickening, and lateral escape with an Indian subcontinent that penetrates further into Eurasia [e.g., *Dewey and Burke*, 1973; *England and McKenzie*, 1982; *Vilotte et al*., 1982; *Tapponnier et al*., 1982]. (3) Continental Injection involves the introduction of Indian crust plunging into lower crust of Tibet as a grand hydraulic piston, transmitting pressure to the base of brittle upper crust throughout Tibet, leading to uplift of the plateau [*Zhao and Morgan*, 1987]. (4) Convective Removal of Mantle Lithosphere, one of the deepest geophysical models, supposes the evolution in elevation is a three-stage process: (a) When the mean elevation of the plateau rises to a certain height because of the crustal thickening caused by India's penetration into Eurasia, the mantle lithosphere will also thicken and protrude downward to form a "lithospheric root" to isostatically compensate the crustal thickening; (b) When the relatively cold, dense lower lithospheric root pushes into the hotter asthenosphere, it will become gravitationally unstable and will cause convective instability of the thickened mantle

lithosphere. With the growth of such instability and associated removal of part or all of the mantle lithosphere root, it will thin the lithosphere and will relieve the loading on the asthenosphere. As a result, the neutral buoyancy force will cause a supplemental uplift of the Tibetan Plateau for awhile; (c) With the further removal and thinning of the mantle lithosphere, the divergence of the surrounding lithosphere will eventually cause horizontal extension and thinning of the crust and thus subsidence of the plateau [*Molnar et al*., 1993].

[25] *Li and Fang* [1998] and *Li et al*. [2001] synthesized various survey data of many kinds and concluded that the Tibetan Plateau had undergone a remarkable uplift of more than 1000 m in late Eocene (~40 Ma) and late Miocene (~20 Ma), respectively, and fell to some extent by peneplanation later. But it rose again rapidly after 4 Ma B.P. to reach its present altitude. Recently, *Rowley and Currie* [2006] declared that the plateau had reached its present altitude at least 35 Ma ago, based on stable isotope-based paleo-altimetry, and claimed that their results disproved the mantle-thickening model (i.e., the model of convective removal of mantle lithosphere) of *Molnar et al*. [1993] for the formation of the plateau. However, *Molnar et al*. [2006], using the same data from *Rowley and Currie*'s work [2006], argued that the data offer strong support for the idea that convective removal of the mantle lithosphere contributed to the unusual height of the present-day Tibetan Plateau; that in the first 10 Ma, the horizontal shortening of the lithosphere from the convergence of India-Eurasia was enough to have doubled the crustal thickness of the plateau and produced a high elevation comparable with the present day. Then, convective removal of mantle lithosphere material and the neutral buoyancy force from asthenosphere made a rapid, supplemental uplift that happened at least 35 Ma ago, pushing the plateau even higher than today. Then, with the further removal and thinning of the mantle lithosphere, the divergence of the surrounding lithosphere caused horizontal extension and thinning of the crust, and thus, a series of NS striking normal faults have developed in southern Tibet since 8 ~ 15 Ma B.P. [*Armijo et al*., 1986; *Chen et al*., 2004].

[26] In our results in Figure 6, we see an obvious weak uplift rate or even subsidence in the middle southern plateau of low-relief surface and high elevation of ~4500 m, which means a process of tremendous tectonic uplift had occurred before and followed by mountain range erosion and basin filling [*Liu et al*., 2006]. The subsiding area in the middle southern plateau is about 750 thousand km^2, and well colocated with the endorheic region of the plateau, where more than 1000 lakes are distributed [*Zhang et al*., 2013]. In the last 10 years, both Ice, Cloud, and land Elevation Satellite (ICESat) elevations and gravity field map from Gravity Recovery and Climate Experiment (GRACE) have revealed significant mass increase in the area, resulting from the increased supply of surface water, perhaps due to global warming [*Zhang et al*., 2011a; *Jacob et al*., 2012]. As we know, migration of land water can cause redistribution of surface loads and thus leads to an instantaneous deformation response in the elastic crust. *Fu and Freymueller* [2012] calculated the vertical deformation in the Himalayan ranges caused by the migration of land water, based on GRACE data, and found that the deformation was at the level of 0.5–1 mm/yr over the whole region. Considering that the amount of mass change in the endorheic region of the middle southern plateau is less than that of Himalayan range, we can infer that the vertical nontectonic deformation in this area caused by land-water variation is less than 1 mm/yr, which means that the subsiding rates of between 0 and −3 mm/yr in this region, derived from GPS observations, are mainly attributed to tectonic deformation. In fact, the widely developed NS striking normal faults in this area, as well as the overall topography as a basin, also demonstrates that subsidence in this area did not initiate in present day but rather is a continuation of neotectonic movement.

[27] In the northeastern margin of the plateau, our GPS results showed that the uplift difference between the Qilian Shan and its piedmont basin, the Hexi Corridor basin, is about 1 mm/yr. *Cui et al*. [2009] obtained an identical result of 1.2 mm/yr using leveling observations taken between 1972 and 2000. Similarly, in the eastern margin of the plateau, our GPS results revealed that the uplift difference between the plateau and its piedmont basin, the Sichuan basin, is more than 4 mm/yr, which also agrees with leveling results in this area [*Wang et al*., 2008b]. The agreement is especially good in the Longmen Shan and Gongga Shan areas, where both GPS and leveling demonstrate localized high uplift rates in these two mountain areas. These convinced us that our vertical velocity field of the Tibetan Plateau inferred from GPS measurements is correct.

[28] Geological findings suggest that the neotectonic deformation in the western part of the northeastern plateau is mainly characterized by horizontal shortening, in accordance with a series of imbricate thrust faults and active folds [*Zhang et al*., 2004], whereas the eastern part of the northeastern plateau is characterized by clockwise rotation, supported by the development of a series of arc-shaped left-lateral strike slip and thrust faults [*Xu et al*., 1994]. The difference in tectonic style and crustal deformation between the eastern and western sections is also reflected in our GPS vertical velocity field. That is, the eastern region has a gentler gradient in the decrease of vertical rate than the western (Figures 7a and 7c). *Zhang et al*. [2006] proposed that the northeast margin of plateau has been undergoing a recent round of growth and rise since the 5–8 Ma B.P. in late Cenozoic and concluded that the horizontal velocity field of the Qilian Shan subregion has been stable recently, based on the evidence that the convergence rate between the Qaidam and Alashan blocks from GPS is consistent with geological results. If that conclusion is true, and further assuming that the vertical velocity field is also stable, we can estimate that the accumulated rise in the Qilian Shan subregion is about 5000 m in the past 5 Ma with an average uplift rate of ~1 mm/yr like present day (Figure 7a). This estimate is generally consistent with the present surface elevation of ~4400 m (Figure 7a), taking into consideration the preexisting mountain base and erosion.

[29] The southeast corner of the Tibetan Plateau has a terrain that gradually decreases in elevation along SE direction (Figure 7d). *Clark and Royden* [2000] explained that this kind of topographic feature results from tilted uplift caused by lower crust flow since Late Miocene. Later, they used a regional, relict landscape in the southeast margin of the plateau to measure vertical deformation and estimated that the vertical rate after Miocene is up to ~0.3 mm/yr in the north of the region and declines to the south [*Clark et al*., 2006]. However, *Hoke et al*. [2008] argued that this area has not significantly uplifted since at least Early Miocene based on stable isotope-based paleo-altimetry. The GPS horizontal

velocity field vividly revealed a glacier-like flow zone that goes clockwise around the Eastern Himalayan Syntaxis and ends at the southeast corner of the plateau with a fanlike front, which could be attributed to an eastward escape of highly plastic upper crustal material driven by a lower crust viscous channel flow [*Gan et al.*, 2007; *Royden et al.*, 2008]. In our GPS vertical velocity field, significant motion difference along the "flow zone" is also revealed, with an apparent trend that the vertical motion is gradually changing from rising in the inner plateau to sinking outside the plateau, with the decrease of terrain height (Figures 6 and 7d).

5. Summary

[30] Based on GPS measurements of 750 stations around the Tibetan Plateau for over 10 years since 1999, we derived a high-resolution 3-D velocity field of present-day crustal movement of the plateau. The GPS data were processed using the software GIPSY/OASIS (Version 6.0) to obtain daily loosely constrained solutions with the Precise Point Positioning (PPP) strategy and JPL products. Station positions and velocities were estimated using the software QOCA, with a sequential Kalman filtering algorithm to adjust all the daily solutions that were transformed into the ITRF2008 reference frame.

[31] The horizontal velocity field of the Tibetan Plateau relative to the Eurasia-fixed reference frame shows that the Indian plate is pushing Eurasia along the Himalayas in NNE direction at a rate of ~40 mm/yr and that the velocity of Tibetan crust slows down sharply from south to north, causing strong shortening between India and Eurasia, as well as an apparent lateral extrusion. Especially in the southeastern plateau, the velocities exhibit conspicuous clockwise rotation around the Eastern Himalayan Syntaxis and present a fanlike front at the southeast corner of the plateau. The velocity pattern explicitly reflects strong lateral extrusion and continuous deformation of the Tibetan upper crust. None of the above main features of the horizontal crustal motion of the plateau demonstrated by our GPS velocity field differs significantly compared with the previous results, although our GPS data have a longer time span.

[32] The vertical velocity field reveals that the Tibetan Plateau is still rising as a whole relative to its stable northern neighbor. However, some regions present insignificant uplift rates or even negative rates. The main features of the vertical crustal deformation of the plateau are the following: (a) The Himalayan ranges is still rising at a rate of ~2 mm/yr, and the uplift rate is ~6 mm/yr with respect to the south foot of Himalayan range; (b) The middle eastern plateau has a typical uplift rate between 1 and 2 mm/yr, and some high mountain ranges in this area, like the Longmen Shan and Gongga Shan, have uplift rates as large as 2–3 mm/yr; (c) In the middle southern plateau, there is a basin and endorheic region with a series of NS striking normal faults, showing obvious sinking with rates between 0 and −3 mm/yr. This seems to support the findings that the middle southern plateau is undergoing a retreat after a rapid supplemental rise in agreement with the model of convective removal of mantle lithosphere; (d) Along a NNE striking profile of the plateau, we can see that the present-day uplifting and sinking regions correspond well with the Cenozoic orogenic belts and basins, respectively; (e) At the southeastern corner of the plateau, while the horizontal velocity field shows an outstanding clockwise rotation and fanlike front of a flow zone, the vertical velocity field also shows significant motion difference from the inner plateau to the outside plateau, with an apparent trend that the uplift rate is gradually decreasing from between 0.8 and 2.3 mm/yr in the inner plateau to between −0.5 and −1.6 mm/yr outside the plateau, with the decrease of terrain height.

[33] Our GPS-derived 3-D velocity field of the Tibetan Plateau can characterize quantitatively the tectonic motion and deformation in the continental collision zone and offer better kinematic constraints for understanding the dynamics of present-day uplift and growth of the plateau.

[34] **Acknowledgments.** The GPS data used in this paper are primarily from the National Key Scientific Projects "Crusta1 Movement Observation Network of China" (CMONOC I) and "Tectonic and Environmental Observation Network of Mainland China" (CMONOC II). We express our gratitude and thanks to all our Chinese participants in constructing the network and making the GPS measurements. This work also used GPS data from the California Institute of Technology and the Institute of Tibetan Plateau Research, Chinese Academy of Sciences, collected in Nepal and southern Tibet. We appreciate their generosity in sharing data with us. We thank our colleague Gao Xianglin for his great help to translate the first drift of this manuscript into English language. We are grateful to William H. Prescott and Zhang Peizhen for their helpful previews of this manuscript. We are particularly indebted to Jeffrey T. Freymueller for his thorough reviews and thoughtful comments which resulted in considerable improvement of this manuscript. This work was supported by the National Science Foundation of China (41174082), the State Key Laboratory of Earthquake Dynamics (LED2012B03), and the Himalaya Project of China Earthquake Administration (201208009).

References

Altamimi, Z., X. Collilieux, and L. Metivier (2011), ITRF2008: An improved solution of the international terrestrial reference frame, *J. Geod.*, *85*, 457–473.

Argand, E. (1924), La tectonique de l'Asie, Proceedings of the VIIIth Intl, *Geol. Cong. Rep. Sess.*, *13*, 170–372.

Armijo, R., P. Tapponnier, L. Mercier, and T. Han (1986), Quaternary extension in southern Tibet: Field observations and tectonic implications, *J. Geophys. Res.*, *91*, 13,803–13,872.

Beavan, J., P. Denys, M. Denham, B. Hager, T. Herring, and P. Molnar (2010), Distribution of present-day vertical deformation across the Southern Alps, New Zealand, from 10 years of GPS data, *Geophys. Res. Lett.*, *37*, L16305, doi:10.1029/2010GL044165.

Blewitt, G. (2008), Fixed point theorems of GPS carrier phase ambiguity resolution and their application to massive network processing: Ambizap, *J. Geophys. Res.*, *113*, B12410, doi:10.1029/2008JB005736.

Boehm, J., A. Niell, P. Tregoning, and H. Schuh (2006), Global Mapping Function (GMF): A new empirical mapping function based on numerical weather model data, *Geophys. Res. Lett.*, *33*, L07304, doi:10.1029/2005GL025546.

Chen, Q., J. Freymueller, Q. Wang, Z. Yang, C. Xu, and J. Liu (2004), A deforming block model for the present-day tectonics of Tibet, *J. Geophys. Res.*, *109*, B01403, doi:10.1029/2002JB002151.

Chung, S.-L., C.-H. Lo, T.-Y. Lee, Y. Zhang, Y. Xie, X. Li, K.-L. Wang, and P.-L. Wang (1998), Diachronous uplift of the Tibetan plateau starting 40 Myr ago, *Nature*, *394*, 769–773.

Clark, M., and L. Royden (2000), Topographic ooze: Building the eastern margin of Tibet by lower crustal flow, *Geology*, *28*, 703–706.

Clark, M., L. Royden, K. Whipple, B. C. Burchfiel, X. Zhang, and W. Tang (2006), Use of a regional, relict landscape to measure vertical deformation of the eastern Tibetan Plateau, *J. Geophys. Res.*, *111*, F03002, doi:10.1029/2005JF000294.

Cui, D., Q. Wang, Y. Hu, W. P. Wang, and W. F. Liang (2009), Lithosphere deformation and deformation mechanism in northern margin of Qinghai-Tibet plateau (in Chinese), *Chinese J. Geophys.*, *52*, 1490–1499.

Deng, Q., P. Zhang, Y. Ran, X. Yang, W. Min, and Q. Chu (2003), Basics characteristics of active tectonics of China, *Sci. China*, *46*(4), 356–372.

Devoti, R., G. Pietrantonio, A. R. Pisani, F. Riguzzi, and E. Serpelloni (2010), Present day kinematics of Italy, in *J. Virtual Explorer*, edited by M. Beltrando et al., *36*, paper 2, doi:10.3809/jvirtex.2010.00237.

Dewey, J., and K. Burke (1973), Tibetan, Variscan, and Precambrian basement reactivation: Products of continental collision, *J. Geol.*, *81*, 683–692.

Dong, D., T. Herring, and R. King (1998), Estimating regional deformation from a combination of space and terrestrial geodetic data, *J. Geod.*, *72*, 200–214.

Dong D., P. Fang, Y. Bock, F. Webb, L. Prawirodirdjo, S. Kedar, and P. Jamason (2006), Spatiotemporal filtering using principal component analysis and Karhunen-Love expansion approaches for regional GPS network analysis, *J. Geophys. Res.*, *111*, B03405, doi:10.1029/2005JB003806.

England, P., and G. Houseman (1989), Extension during continental convergence with special reference to the Tibetan plateau, *J. Geophys. Res.*, *94*, 17,561–17,597.

England, P., and D. McKenzie (1982), A thin viscous sheet model for continental deformation, *Geophys. J. Int.*, *70*, 295–321.

Farrell, W. E. (1972), Deformation of the Earth by surface loads, *Rev. Geophys. Space Phys.*, *10*(3), 761–797.

Fu, Y., and J. Freymueller (2012), Seasonal and long-term vertical deformation in the Nepal Himalaya constrained by GPS and GRACE measurements, *J. Geophys. Res.*, *117*, B03407, doi:10.1029/2011JB008925.

Fu, Y., J. Freymueller, and T. van Dam (2012), The effect of using inconsistent ocean tidal loading models on GPS coordinate solutions, *J. Geod.*, *86*(6), 409–421.

Gan, W., P. Zhang, Z.-K. Shen, Z. Niu, M. Wang, Y. Wan, D. Zhou, and J. Cheng (2007), Present-day crustal motion within the Tibetan Plateau inferred from GPS measurements, *J. Geophys. Res.*, *112*, B08416, doi:10.1029/2005JB004120.

Gan, W., et al. (2012), Construction and application of tectonics and environmental observation network of mainland China (in Chinese), *J. Eng. Stud.*, *4*, 324–331.

Harrison, T. M., P. Copeland, W. S. F. Kidd, and O. Lovera (1995), Activation of the Nyainquentanghla shear zone: Implications for uplift of the southern Tibetan Plateau, *Tectonics*, *14*, 658–676.

Hoke, G., C. Garzione, and L. Chen (2008), Stable isotopic records from Cenozoic basins in the SE Margin of the Tibetan Plateau, Yunnan Province, China: Implications for regional paleoelevation, American Geophysical Union, Fall Meeting 2008.

Jacob, T., J. Wahr, W. Tad Pfeffer, and S. Swenson (2012), Recent contributions of glaciers and ice caps to sea level rise, *Nature*, *482*, 514–518.

Jiang, G., C. Xu, Y. Wen, Y. Liu, Z. Yin, and J. Wang (2013), Inversion for coseismic slip distribution of the 2010 Mw 6.9 Yushu Earthquake from InSAR data using angular dislocations, *Geophys. J. Int.*, doi:10.1093/gji/ggt141.

Kapp, P., and J. Guynn (2004), Indian punch rifts Tibet, *Geology*, *32*, 993–996.

Lee, H.-Y., S.-L. Chung, and S.-L. Wang (2003), Miocene Jiali faulting and its implications for Tibetan tectonic evolution, *Earth Planet. Sci. Lett.*, *205*, 185–194.

Li, J., and X. Fang (1998), Research on Tibetan plateau uplift and the change of environments (in Chinese), *Chinese Sci. Bull.*, *43*, 1569–1674.

Li, J., X. Fang, B. Pan, Z. Zhao, and Y. Song (2001), Late Cenozoic intensive uplift of Qinghai-Xizang Plateau and its impacts on environments in surrounding area (in Chinese), *Quat. Sci.*, *9*, 281–391.

Liu, J., L. Ding, L. Zeng, T. Paul, and G. Yves (2006), Large-scale terrain analysis of selected regions of the Tibetan plateau: Discussion on the origin of plateau planation surface (in Chinese), *Earch Sci. Front.*, *13*, 285–299.

Ma, R., et al. (2011), China's lakes at present: Number, area and spatial distribution, *Sci. China*, *54*(2), 283–289.

McCaffrey, R., and J. Nabelek (1998), Role of oblique convergence in the active deformation of the Himalayas and southern Tibet plateau, *Geology*, *26*, 691–694.

Molnar, P., and P. Tapponnier (1975), Cenozoic tectonics of Asia: Effects of a continental collision, *Science*, *189*, 419–426.

Molnar, P., P. England, J. Martinod, and M. Dynamics (1993), Uplift of the Tibetan Plateau, and the Indian Monsoon, *Rev. Geophys.*, *31*, 357–396.

Molnar, P., G. Houseman, and P. England (2006), Palaeo-altimetry of Tibet, *Nature*, *444*, E4.

Niu, Z., et al. (2005), Contemporary velocity field of crustal movement of Chinese mainland from Global Positioning System measurements, *Chin. Sci. Bull.*, *50*(9), 939–941.

Okada, Y. (1992), Internal deformation due to shear and tensile faults in a half-space, *Bull. Seismol. Soc. Am.*, *82*, 1018–1040.

Powell, C. (1986), Continental underplating model for the rise of the Tibetan Plateau, *Earth Planet. Sci. Lett.*, *81*, 79–94.

Rowley, D. B. (1996), Age of initiation of collision between India and Asia: A review of stratigraphic data, *Earth Planet. Sci. Lett.*, *145*, 1–13.

Rowley, D., and B. Currie (2006), Palaeo-altimetry of the late Eocene to Miocene Lunpola basin, central Tibet, *Nature*, *439*, 677–681.

Royden, L., B. Burchfiel, and R. King (1997), Surface deformation and lower crustal flow in eastern Tibet, *Science*, *276*, 788–790.

Royden, L., B. Burchfield, and R. var der Hilst (2008), The geological evolution of the Tibetan Plateau, *Science*, *321*, 1054–1058.

Scherneck, H. G., J. M. Johansson, and F. H. Webb (2000), Ocean loading tides in GPS and rapid variations of the frame origin, Geodesy Beyond 2000—The Challenges in the First Decade, *Springer*, *121*, 19–30.

Schmid, R., P. Steigenberger, G. Gendt, M. Ge, and M. Rothacher (2007), Generation of a consistent absolute phase-center correction model for GPS receiver and satellite antenna, *J. Geod.*, *81*, 781–798.

Sun, J., Z.-K. Shen, R. Bürgmann, M. Wang, L. Chen, and X. Xu (2013), A three-step maximum a posteriori probability method for InSAR data inversion of coseismic rupture with application to the 14 April 2010 Mw 6.9 Yushu, China, earthquake, *J. Geophys. Res. Solid Earth*, *118*, 4599–4627, doi:10.1002/jgrb.50244.

Tapponnier, P., G. Peltzer, A. Le Dain, R. Armijo, and P. Cobbold (1982), Propagating extrusion tectonics in Asia: New insights from simple experiments with plasticine, *Geology*, *10*, 611–616.

Tapponnier, P., Z. Q. Xu, F. Roger, B. Meyer, N. Arnaud, G. Wittlinger, and Y. Jingsui (2001), Oblique stepwise rise and growth of the Tibet Plateau, *Science*, *294*, 1671–1677.

Thatcher, W. (2007), Microplate model for the present-day deformation of Tibet, *J. Geophys. Res.*, *112*, B01401, doi:10.1029/2005JB004244.

Tregoning, P., and T. van Dam (2005), Atmospheric pressure loading corrections applied to GPS data at the observation level, *Geophys. Res. Lett.*, *32*, L22310, doi:10.1029/2005GL024104.

Tregoning, P., and C. Watson (2009), Atmospheric effects and spurious signals in GPS analyses, *J. Geophys. Res.*, *114*, B09403, doi:10.1029/2009JB006344.

Vilotte, J., M. Daignières, and R. Madariaga (1982), Numerical modeling of intraplate deformation: Simple mechanical models of continental collision, *J. Geophys. Res.*, *87*, 10,709–10,728.

Wan, Y., M. Wang, Z. Shen, J. Chen, Z.-S. Zhang, Q.-L. Wang, and W.-J. Gan (2004), Co-seismic slip distribution of the 2001 west of Kunlun Mountain Pass earthquake inverted by GPS and leveling data, *Seismol. Geol. (in Chinese)*, *26*(3), 394–404.

Wang, Q., et al. (2001), Present-day crustal deformation in China constrained by Global Positioning System measurements, *Science*, *294*, 574–577.

Wang, C. S., X. Zhao, Z. F. Liu, P. C. Lippert, S. A. Graham, R. S. Coe, Haisheng Y., L. Zhu, S. Liu, and Y. Li (2008a), Constraints on the early uplift history of the Tibetan Plateau, *Proc. Natl. Acad. Sci.*, *105*, 4987–4992.

Wang, Q., D. Cui, W. Wang, S. Zhang, J. Liu, and Q. Shi (2008b), Present-day vertical crustal motion in Western Sichuan region (in Chinese), *Sci. China*, *38*, 598–610.

Wang, Q., X. Qiao, Q. Lan, J. T. Freymueller, Y. Shaomin, X. Caijun, Y. Yonglin, Y. Xinzhao, T. Kai, and C. Gang (2011), Rupture of deep faults in the 2008 Wenchuan earthquake and uplift of the Longmen Shan, *Nat. Geosci.*, *4*, 634–640.

Webb, F. H., and J. F. Zumberge (1993), An introduce to GIPSY-OASIS II, Jet Propulsion Laboratory User Manual, JPL Technical Document D-11088, California Institute of Technology.

Xu, X. ,G. Cheng, X. Ma, S. Y., and Han Z. (1994), Rotation model and dynamics of blocks in North China and its adjacent areas, *J China Uni. Geosci. (in Chinese)*, *19*, 129–138.

Xu, Z. Q., J. Yang, and M. Jiang (1999), Continental subduction and uplifting of the orogenic belts at the margin of the Qinghai-Tibet Plateau (in Chinese), *Earth Sci. Front.*, *6*, 139–151.

Yao, T. (2008), Map of Glaciers and Lakes on the Tibetan Plateau and the Surroundings, Xi'an Cartographic Publishing House, Xi'an, China.

Zhang, P., et al. (2004), Continuous deformation of the Tibetan Plateau from Global Positioning System data, *Geology*, *32*, 809–812.

Zhang, P., D. Zheng, G. Yin, Y. Daoyang, Z. Guangliang, L. Chuanyou, and W. Zhicai (2006), Discussion on late Cenozoic growth and rise of northeastern margin of the Tibetan Plateau, *Quat. Sci.*, *26*, 5–13.

Zhang, G., H. Xie, S. Kang, D. Yi, and S. F. Ackley (2011a), Monitoring lake level changes on the Tibetan Plateau using ICESat altimetry data (2003–2009), *Remote Sens. Environ.*, *115*, 1733–1742.

Zhang, G. H., C. Qu, X. Shan, G.-J. Zhang, X. G. Song, R.-J. Wang, Z.-H. Li, and J.-C. Hu (2011b), The coseismic InSAR measurements of 2008 Yutian earthquake and its inversion for source parameters, *Chinese J. Geophys. (in Chinese)*, *54*(11), 2753–2760.

Zhang, G. Q., T. Yao, H. Xie, S. Kang, and Y. Lei (2013), Increased mass over the Tibetan Plateau: From lakes or glaciers?, *Geophys. Res. Lett.*, *40*, 1–6, doi:10.1002/grl.50462.

Zhao, W., and W. Morgan (1987), Injection of Indian crust into Tibetan lower crust: A two-dimensional finite element model study, *Tectonics*, *6*, 489–504.

Zumberge, J. F., M. B. Helfin, D. C. Jefferson, M. M. Watkins, and F. H. Webb (1997), Precise point positioning for the efficient and robust analysis of GPS data from large networks, *J. Geophys. Res.*, *102*, 5005–5017.